JOURNAL OF MAGNETIC RESONANCE IMAGING 12:400–410 (2000)

Original Research

Whole Brain Quantitative CBF, CBV, and MTT Measurements Using MRI Bolus Tracking: Implementation and Application to Data Acquired From Hyperacute Stroke Patients

Anne M. Smith, PhD,* Cécile B. Grandin, MD, Thierry Duprez, MD, Frédéric Mataigne, MD, and Guy Cosnard, PhD

A robust whole brain magnetic resonance (MR) bolus tracking technique based on indicator dilution theory, which could quantitatively calculate cerebral blood flow (CBF), cerebral blood volume (CBV), and mean transit time (MTT) on a regional basis, was developed and tested. T2*-weighted gradient-echo echoplanar imaging (EPI) volumes were acquired on 40 hyperacute stroke patients after gadolinium diethylene triamine pentaacetic acid (Gd-DTPA) bolus injection. The thalamus, white matter (WM), infarcted area, penumbra, and mirror infarcted and penumbra regions were analyzed. The calculation of the arterial input function (AIF) needed for absolute quantification of CBF, CBV, and MTT was shown to be user independent. The CBF values (ml/min/100 g units) and CBV values (% units, in parentheses) for the thalamus, WM, infarct, mirror infarct, penumbra, and mirror penumbra (averaged over all patients) were 69.8 ± 22.2 (9.0 ± 3.0 SD); 28.1 ± 6.9 (3.9 ± 1.2); 34.4 ± 22.4 (7.1 ± 2.7); 60.3 ± 20.7 (8.2 ± 2.3); 50.2 ± 17.5 (10.4 ± 2.4); and 64.2 ± 17.0 (9.5 ± 2.3), respectively, and the corresponding MTT values (in seconds) were 8.0 ± 2.1; 8.6 ± 3.0; 16.1 ± 8.9; 8.6 ± 2.9; 13.3 ± 3.5; and 9.4 ± 3.2. The infarct and penumbra CBV values were not significantly different from their corresponding mirror values, whereas the CBF and MTT values were ($P < 0.01$). Quantitative measurements of CBF, CBV, and MTT were calculated on a regional basis on data acquired from hyperacute stroke patients, and the CBF and MTT values showed greater sensitivity to areas with perfusion defects than the CBV values. J. Magn. Reson. Imaging 2000;12:400–410.

Index terms: bolus tracking; quantitative cerebral perfusion; Gd-DTPA; gradient-echo EPI

SEVERAL GROUPS have reported using MRI bolus tracking methods to measure cerebral blood flow (CBF) and/or cerebral blood volume (CBV) quantitatively (1–4). Using these techniques, a time series of T2*-weighted images is acquired after an IV bolus injection of gadolinium diethylene triamine pentaacetic acid (Gd-DTPA); then measurements of CBF, CBV, and mean transit time (MTT) are made by applying indicator dilution theory (5–7). These values can be quantitative (ie, expressed in absolute units) if the arterial input function (AIF) can be measured. In the groups reporting absolute CBF measurements (1–3), the data were acquired from only a few slices (usually two, one near the base of the skull to image the large arteries and a superior slice). So far, quantitative measurements of CBF, CBV, and MTT for whole brain acquisitions have not yet been reported with MR bolus tracking techniques.

Whole brain acquisitions have several advantages over single-slice acquisitions. First, often clinicians and researchers are not sure of the exact region that is affected by a disease process and therefore do not know a priori which slice or slices need to be imaged. For example, the hyperacute infarct in stroke patients can be delineated with diffusion imaging, but the actual three-dimensional (3D) extent of the penumbra is not known, and the whole brain should be imaged to be sure that it is completely covered. Second, whole-brain acquisitions can be easily coregistered to other volumes acquired during the same session or on different days, which is difficult to do with single-slice data. Finally, the calculation of the AIF that is necessary for absolute quantification is more flexible. More voxels can be used for the calculation and arteries near the region of interest can be chosen, thereby reducing the effects of dispersion (not done in this study).

The purpose of this study was to implement indicator dilution theory on dynamically acquired whole brain gradient-echo echoplanar imaging (EPI) volumes after Gd-DTPA injection. The technique we developed for estimating the AIF from an entire brain volume is explained and shown to be user independent. This technique can be applied to normal volunteers as well as patients with various types of neurologic disorders (eg, degenerative diseases, epilepsy, and stroke), for whom regional quantitative measures of CBF, CBV, and MTT are desired from whole brain data. Performing absolute

Department of Radiology and Medical Imaging, Université Catholique de Louvain, St. Luc University Hospital, B-1200 Brussels, Belgium.

*Address reprint requests to: A.M.S., Department of Radiology and Medical Imaging, Université Catholique de Louvain, Cliniques Universitaires Saint Luc, Avenue Hippocrate 10, B-1200 Brussels, Belgium. E-mail: Smith@topo.ucl.ac.be

Received March 6, 2000; Accepted April 10, 2000.

quantification allows for an easier comparison between subjects and follow-up studies on the same subject. The technique was retrospectively applied to data acquired from hyperacute stroke patients to demonstrate the type of information a whole brain quantitative technique can provide about the CBF, CBV, and MTT absolute values of infarct, penumbra, and corresponding mirror regions. How these values impact hyperacute stroke patient management and predict eventual infarction of penumbra is currently being investigated and will not be presented in this paper, although two extreme cases will be presented in detail and some preliminary results given.

MATERIALS AND METHODS

Implementation of Indicator Dilution Theory

In order to use indicator dilution theory, MR signal intensity must be converted to Gd concentration (8–11):

$$C_m(t) = -K \cdot \ln \frac{S(t)}{S_o}, \quad (1)$$

where $C_m(t)$ is the measured concentration of Gd-DTPA with respect to time, K is a proportionality constant that is inversely proportional to the TE and depends on the MR scanner, $S(t)$ is the MRI signal intensity with respect to time, and S_o is the baseline MRI signal before the presence of Gd-DTPA and after a steady-state magnetization has been achieved. Since the same TE was used when acquiring all slices of the bolus tracking volumes and assuming that each tissue type (eg, large and small vessels) will have the same proportionality constant [which is not true for a spin echo EPI sequence (12,13)], the actual value of K was never estimated since it cancels out (see equations below). We used three images (second, third, and fourth acquired bolus tracking volumes) to calculate S_0. In our implementation, $C_m(t)$ could be calculated on an ROI basis as well as a voxel-by-voxel basis.

Indicator dilution theory can be applied to MR bolus tracking images to quantify CBF, CBV, and MTT. When an ideal instantaneous arterial bolus (ie, a delta function) of Gd-DTPA is the input to a tissue region, the following relation exists between the parameters (5,6,14):

$$\frac{\text{CBV}}{\text{CBF}} = \frac{\int C(t)dt}{C_{\max}}, \quad (2)$$

where $C(t)$ is the concentration of Gd-DTPA in a tissue region and C_{max} is the maximum of this curve. However, an instantaneous arterial bolus is not possible in practice but $C(t)$ (the tissue response to an instantaneous arterial bolus) can be calculated using the relation:

$$C(t) = C_m(t) \otimes^{-1} \text{AIF}(t) \quad (3)$$

where $C_m(t)$ is the measured tissue curve, AIF(t) is the measured AIF curve, and $\otimes^{-1}$ represents the deconvolution operation. Absolute CBV can be calculated as:

$$\text{CBV} = \frac{\kappa}{\rho} \cdot \frac{\int C_m(t)dt}{\int \text{AIF}(t)dt}, \quad (4)$$

where $\kappa = (1 - \text{HCT}_{LV})/(1 - \text{HCT}_{SV})$ corrects for the fact that the hematocrit in large vessels (HCT_{LV} was set to 0.45) is larger than the hematocrit of small vessels (HCT_{SV} was set to 0.25) (1), and ρ is the density of brain tissue (1.04 g/ml) (7). Once $C(t)$ and CBV using Eqs. [3] and [4] have been calculated, CBF can be calculated using Eq. [2]. Finally, the MTT can be calculated using the following relation (5):

$$\text{MTT} = \frac{\text{CBV}}{\text{CBF}} \quad (5)$$

Determination of the AIF

A program was developed to allow interactive selection of voxels located in major brain arteries (Fig. 1). This was done by searching for voxels that had an early and large increase in Gd-DTPA concentration. The program first selected those voxels whose peak Gd-DTPA concentration value was above 60% of the maximum voxel Gd-DTPA concentration in the entire time series volumes and whose peak value fell between a time window of 3 and 30 seconds. Hundreds of voxels were usually selected in this initial pass, and an average AIF was calculated from these selected voxels. The selected voxels were superimposed in red on top of the first bolus tracking volume (displayed in black and white). The user could then step through the slices and select by clicking with the mouse those voxels most likely belonging to an artery (such as the basilar, carotid, or middle cerebral arteries), and the Gd-DTPA concentration time curve was displayed for that particular voxel. Once the user was satisfied that a selected voxel was indeed an artery, he/she decreased the time window such that only a single time point was contained within the window, and then the average AIF was recalculated. The height threshold was then raised until only 20 or so voxels remained in the average AIF, and finally the user inspected each of the remaining voxels and could exclude noisy voxels or voxels not likely located in an artery. Seven to 15 voxels were usually averaged to calculate the final AIF for each patient. No attempt was made to select voxels near the tissue ROI being analyzed, and no correction for dispersion of the AIF during travel to the tissue ROI was made.

To test interobserver variability of AIF calculation, four trained radiologists independently calculated an AIF for each patient. The CBF, CBV, and MTT for two tissue ROIs (parietal cortex and centrum semioval) were calculated using the four different AIFs for each patient, and a one-way analysis of variance (ANOVA) was used to test for significant differences between the CBF and CBV values calculated from the four different AIFs.

Gamma Variate Fitting

Gamma variate fitting was used to denoise the data and correct for tracer recirculation (1,3,4). The fitting in this study was implemented both on a voxel-by-voxel basis and on a region-of-interest (ROI) basis. The AIF(t) and

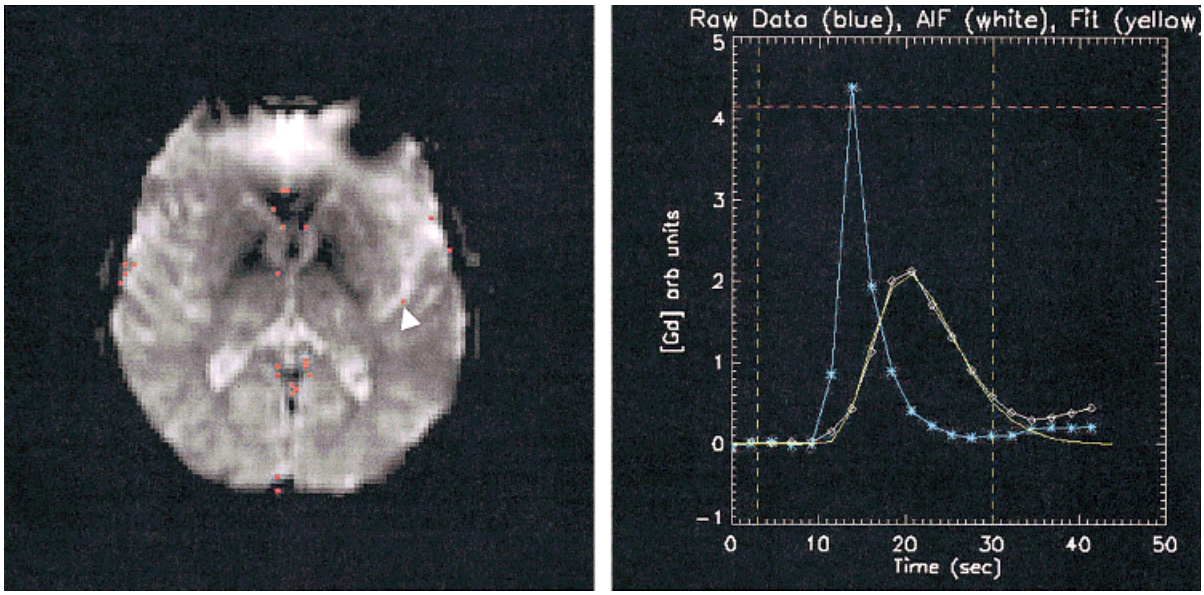

Figure 1. AIF calculation widget showing results of initial AIF calculation. Note that venous voxels were included in this initial pass. The height threshold was set to 0.60 (60% of the maximum value of all bolus tracking volumes), and the time window was set to 3–30 seconds (arterial peak minimum and maximum). After this initial pass, 600 voxels were included in the averaged AIF curve (white curve in graph, with the gamma variate fit shown in yellow). The blue curve in the graph represents the voxel next to the white arrow and is most likely located in the middle cerebral artery. The next step would be to decrease the time window (vertical yellow broken lines in the graph) such that it only contains the peak of the blue curve and increase the height threshold (horizontal broken red line in the graph) such that only approximately 20 voxels remain. The user can view each voxel individually and exclude the unwanted voxels for the final calculation of the AIF.

tissue $C_m(t)$ curves were both fit to a gamma variate function using the Levenberg-Marquardt method (15,16):

$$\mathrm{AIF}_{\mathrm{fit}}(t) \text{ or } C_{\mathrm{fit}}(t) = -K(x-\Delta)^{\alpha} \cdot e^{-(x-\Delta)/B} \cdot F_{\mathrm{step}}(x-\Delta), \quad (6)$$

where $\mathrm{AIF}_{\mathrm{fit}}(t)$ and $C_{\mathrm{fit}}(t)$ are the fitted AIF(t) and $C_m(t)$ curves, respectively, K is a constant, x is the image number, Δ is the delay between image 0 and the arrival of the bolus (a positive number), α and B are gamma variate parameters, and F_{step} is a step function defined by:

$$F_{\mathrm{step}} = \begin{cases} 1 & \text{for } (x-\Delta) \geq 0 \\ 0 & \text{for } (x-\Delta) < 0 \end{cases}. \quad (7)$$

All data points were assigned a weight of 1.0 during the fitting process. To eliminate the effects of recirculation, any time points that were less than 30% of the maximum after the peak of the AIF(t) and $C_m(t)$ curves were not used in the fit. In some regions with delayed bolus passage (such as infarcted regions), the 30% threshold was too low, and the user could increase the threshold until the X^2 value of the gamma variate fit was within ±10% of the value from the healthy mirror region.

MRI Protocol

Forty patients with confirmed brain infarct were selected from a larger population of patients who had suspected stroke. All patients in the large population had undergone an MRI study within 6 hours of symptom onset, and only patients (or relatives) who could state the time of symptom onset exactly were included in the study. The MRI protocol included a T1-weighted whole brain sagittal sequence (to detect a possible hemorrhage since no computed tomography scanning was performed), a fast spin-echo T2-weighted sequence (to detect lesions in the brainstem), a fast fluid-attenuated inversion recovery sequence [FLAIR, to detect nonacute lesions and occluded vessels (17)], a 3D time-of-flight angiography sequence (to detect occluded vessels or slow flow since no computed tomography angiography was performed), a diffusion-weighted sequence (to detect hyperacute lesions), and a bolus tracking perfusion-weighted sequence. The total time in the scanner for each patient was less than 30 minutes, which also gave the neurologist time to contact relatives for possible thrombolytic therapy consent since it was not an approved therapy in Belgium at the time of the study. Since the data analysis was performed only on the diffusion-weighted and bolus tracking volumes, only these sequences will be described in further detail.

All imaging was performed using a 1.5-T GE Signa scanner (GE Medical Systems, Milwaukee, WI) with 5 mm slice thickness, 0.5 mm interslice gap, 24×24 cm^2 field of view (FOV), and 24 slices per volume. A diffusion trace volume (to delineate new infarcts) was calculated from three diffusion-weighted volumes with the diffusion gradients applied along each of the x, y, and z directions, respectively. These volumes were acquired using a spin-echo EPI sequence (TR/TE 4500/95 msec, 128×128 matrix, b = 1000 s/mm^2, δ = 32 msec, and Δ = 39 msec, where δ represents the length of time that a single diffusion-sensitizing gradient was on, and Δ

represents the time between the start of the first diffusion-sensitizing gradient and the start of the second one).

A single-shot gradient-echo EPI sequence (TR/TE 2.3 sec/30 msec) was used to perform the bolus tracking, with the sequence started either at the same time or a few seconds after the Gd-DTPA injection (0.1 mmol/kg). The bolus was injected at a rate of 10 ml/sec in an antecubital vein by an MRI power injector (Medrad, Pittsburgh, PA) followed by a 30-ml saline flush. A 128×96 acquisition matrix was used, and 20 volumes were acquired over time. Therefore, the entire brain was imaged every 2.3 seconds for 46 seconds after injection of Gd-DTPA.

No smoothing was performed on any of the images. The diffusion and bolus tracking images were acquired without moving the patient between the scans. The first acquired bolus tracking volume was used only for registration and display purposes since it was not in steady-state magnetization, and time 0 in our study was assigned to the second acquired volume; therefore 43.7 seconds was assigned to the 20th acquired volume. One to 5 days after the initial examination, follow-up FLAIR images ($TR/TE_{eff}/TI$ 10 sec/159 msec/2200 msec, 256×160 acquisition matrix) were acquired for each patient for positive confirmation of stroke.

Correction for Patient Movement

All images were transferred to an offline workstation (Sun Ultra 1/200, Sun Microsystems, Mountain View, CA) for processing using programs written in C and IDL (Research Systems, Boulder, CO). A registration (18) was performed when anatomically drawn contours on the diffusion images did not match the anatomy of the first bolus tracking volume. Patient movement during the acquisition of the 20 bolus tracking volumes was detected by playing a cine loop of the same slice with respect to time. If movement greater than approximately 1 voxel was detected, each bolus tracking volume was registered to the first acquired bolus tracking volume. The follow-up FLAIR images were registered and resampled to the position and size of the first acquired bolus tracking volume.

Data Analysis

Quantitative maps of the CBF, CBV, MTT, bolus arrival time (BAT), and time to peak (TTP) were calculated on a voxel-by-voxel basis. First, voxel-by-voxel fits of the $C_m(t)$ curves to the gamma variate function (Eq. [6]) were performed, and then the fits were deconvolved using Eq. [3]. Equations [2], [4], and [5] were then implemented on a voxel-by-voxel basis to calculate the CBF, CBV, and MTT maps, respectively. The BAT was the time between the peak of the AIF and 10% of the maximum of $C_m(t)$, and similarly the TTP was the time between the peak of the AIF and the peak of $C_m(t)$. A sixth calculated volume (MAX) was formed by taking the maximum of the deconvolved $C(t)$ curves. Only those voxels whose signal intensity on the first bolus tracking volume was greater than 10% of the maximum of this volume were used to create the maps in order to exclude voxels outside the brain and within the susceptibility artifact regions. The average and standard deviation of the CBV volume map were calculated, and those voxels that had a CBV value greater than 2 standard deviations from the average were excluded from further analysis since these voxels were most likely large vessels.

Seven 3D ROIs were drawn for each patient. Three ROIs were drawn on the contralateral side with respect to the infarcted areas in the thalamus, parietal cortex, and centrum semiovale on the first volume of the bolus tracking images. A trained radiologist outlined the hyperintense signal area (corresponding to the infarct) on the diffusion trace volume, and this ROI was called the infarcted ROI; the same radiologist placed an ROI on the abnormally long (with respect to the contralateral side) MTTs on the calculated MTT volume. The difference between this ROI and the infarcted MRI was calculated and called the "penumbra" ROI. For the purposes of this paper, penumbra refers to the region (not including the infarcted region) that has an abnormally long MTT with respect to the mirror contralateral side. The final two ROIs were the contralateral mirror ROIs of the infarcted and penumbra regions. The ROIs from 10 patients were placed on the CBF and CBV volume maps to obtain an average and standard deviation of the CBF and CBV [ie, when $C_m(t)$ was calculated on a voxel-by-voxel basis]. These values were compared with the corresponding values from the region analysis [ie, when $C_m(t)$ was calculated on a regional basis] to determine whether an ROI analysis is equivalent to placing the same ROI on voxel-by-voxel calculated maps.

Statistical Analysis

A two-sample *t*-test assuming unequal variances was used to determine whether significant differences existed between the GM CBF, CBV, and MTT values and their corresponding WM values, and between the infarcted and penumbra values and their corresponding mirror values. In addition, the MTT values for all regions were compared with the WM MTT value, and the *P* value was multiplied by 5 to correct for multiple tests. A *P* value of less than 0.05 was considered significant. Signal-to-noise ratios (SNRs) were calculated for two different bolus tracking volumes for a single patient for the six ROIs. The second acquired volume (a baseline volume) and the volume that displayed the peak signal decrease for the given ROI were used for SNR calculation, using the following formula: SNR = (mean signal intensity of ROI)/(standard deviation of a background ROI). The value ζ, a factor that incorporates noise due to the logarithm calculation of Eq. [1], was also calculated for a single patient using the formula (19):

$$\varsigma = \frac{S_o^2}{N} \sum_{i=1}^{N} \frac{1}{S_i^2}, \qquad (8)$$

where S_0 is defined as for Eq. [1], N are the number of images used for the gamma variate fit for the given region, and S_i is the average signal intensity of the given region for the ith time point.

RESULTS

In data from 2 of the 40 patients scanned, the arterial bolus was delayed (the peak of the AIF occurred after 25.3 seconds) such that the tissue $C_m(t)$ curves were severely truncated and could not be used for further analysis. Both patients had a history of cardiac disorders, with one having atrial fibrillation and mitral valve regurgitation and the other having chronic cardiac insufficiency. In data from the remaining 38 patients, the average time of the AIF peak occurred at 14.3 ± 4.1 seconds (range 6.9–23 seconds). In data from one patient, the AIF peak was early (6.9 seconds), and therefore only two images were used to calculate the baseline signal intensity S_0 (Eq. [1]) instead of the usual three. The series of bolus tracking volumes from two patients had to be registered to the last bolus tracking volume due to patient movement during the acquisition. In data from one patient, no abnormal hyperintense signal was seen on the trace diffusion volume, and thus no infarct ROI and its corresponding mirror ROI could be drawn. In data from nine patients, no abnormal MTT regions were seen on the calculated MTT volume and thus no penumbra ROIs and their corresponding mirror ROIs existed for these patients.

The gamma variate fit failed (ie, the X^2 value was not within ±10% of the healthy mirror regions) for three infarcted regions and one penumbra region where there was not sufficient bolus passage, and these regions were excluded from the study. The cutoff threshold for the gamma variate fit had to be adjusted by the user for 13 infarcted and penumbra regions. A total of 206 ROIs were analyzed and compared. The average volume of the infarcted regions was 26.3 cm^3 (range 0.14–248.0 cm^3, not including the patients in whom no infarct was seen) and the average volume of the penumbra regions was 51.6 cm^3 (range 0.32–189.0 cm^3, not including regions from the nine patients in whom no abnormal MTT was seen outside of the infarct). Figure 2A shows a typical AIF and its gamma variate fit from a single patient, and Fig. 2B shows the $C_m(t)$ curves from the infarcted and mirror infarcted regions and their respective gamma variate fits.

In Figure 3, all the calculated map images, the diffusion-weighted trace image, and the follow-up FLAIR image acquired more than 24 hours after symptoms onset are displayed from the same patient and the same slice level. In all calculated maps, voxels that could not be fit to the gamma variate function were assigned a value of 0 (and hence are black in the figure). Note that the BAT, TTP, and MTT give qualitatively the same map, with the BAT map being slightly noisier. This was typical in all of our studies. The MAX map was very similar to the CBF map, which was expected since they are proportional to each other (Eq. [2]). The MTT map showed abnormally long mean transit times for a region larger than the infarct (infarct was defined on the diffusion trace image and confirmed on the follow-up FLAIR image), and this region minus the infarcted region was defined to be the penumbra.

Table 1 summarizes the statistics for the four different sets of AIFs calculated by the different radiologists for all 40 patients.Figure 4A–C shows the interobserver

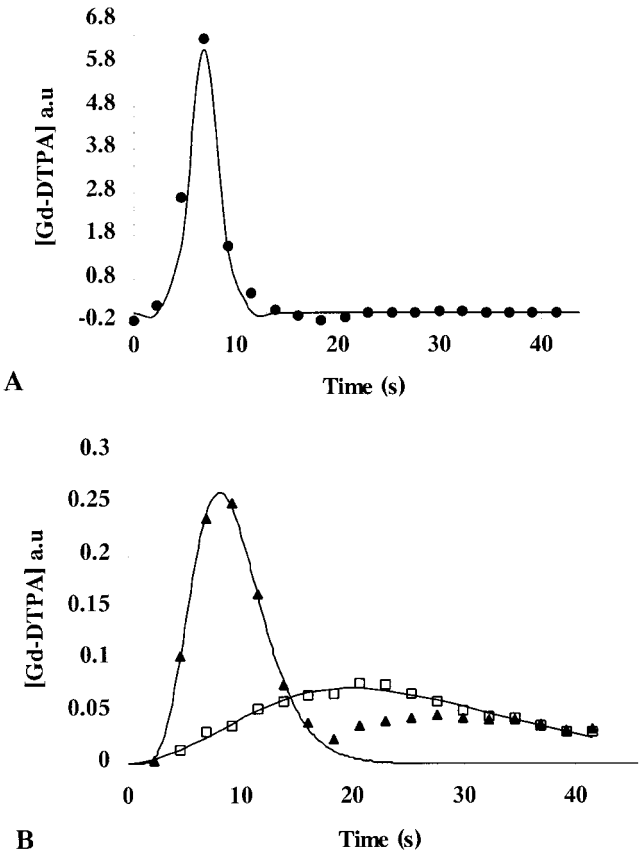

Figure 2. **A:** AIF curve (circles) and gamma variate fit (solid line) from a single patient (X^2/df = 0.18, where df are the degrees of freedom of the fit). This AIF was the average of 9 voxels. **B:** Infarcted region $C_m(t)$ curve (boxes) with gamma variate fit (X^2/df = $1.0e^{-4}$) superimposed (solid line) and mirror infarcted region $C_m(t)$ curve (triangles) with gamma variate fit (X2/df = $9.9e^{-5}$) superimposed (solid line). Regions are from the same patient as in A. Note that the values for the X^2/df are dependent on the region since an unweighted gamma variate fit was used.

variability among the four different AIF curves used to calculate the CBF, CBV, and MTT for the WM and GM ROIs for each of the 38 patients. There were no statistically significant differences among the four observers for any of the data shown in Fig. 4 when the ANOVA analysis was performed ($P > 0.75$).

Table 2 displays the average and standard deviations of the CBF, CBV, and MTT from all the patients for six different anatomical regions.The four ROIs for which the gamma variate fit failed were not included in these averages. Note that the MTT values for the thalamus, mirror infarct, and mirror penumbra regions compared with the MTT values for the WM were not significantly different, while there were significant differences between the WM MTT values and the infarct and penumbra region values. Also note that no significant differences existed between the infarct and penumbra CBV values and their corresponding mirror CBV values, while the CBF values did demonstrate significant differences.

Table 3 summarizes the results of the ROI analysis for 10 patients compared with the same ROI drawn on

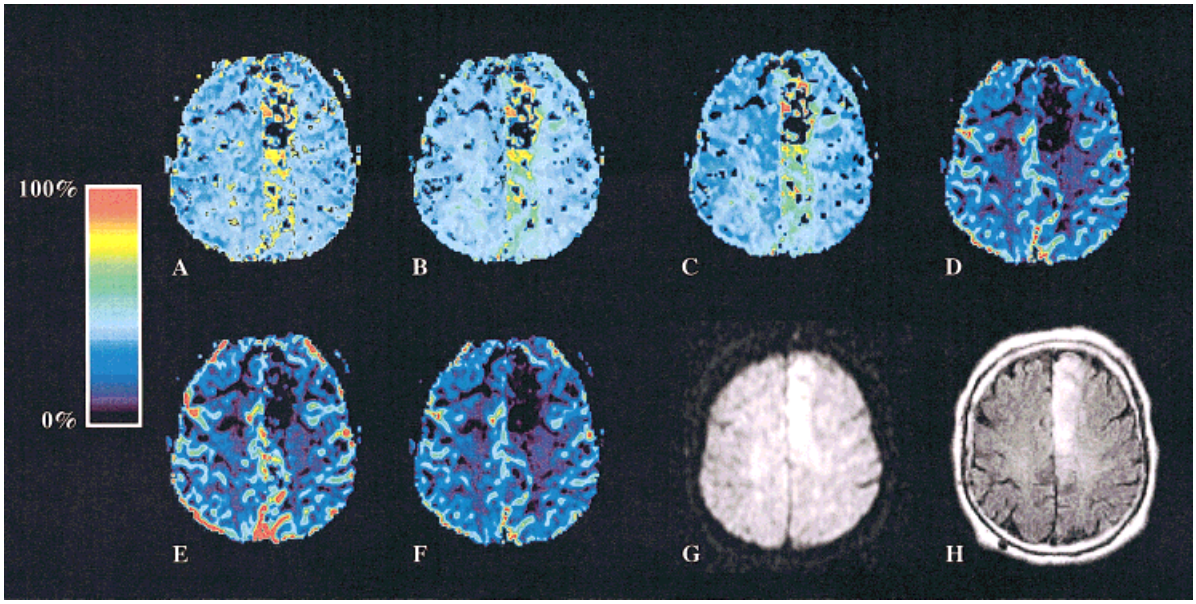

Figure 3. Single slice from same patient who had an infarct in the left anterior cerebral artery territory showing the BAT map (**A**), TTP map (**B**), MTT map (**C**), MAX map (**D**), CBV map (**E**), CBF map (**F**), diffusion trace image (**G**), and the follow-up FLAIR image (**H**) more than 24 hours after stroke onset. The calculated maps use the color scale on the left of the figure. The affected area is clearly visible on all the images.

the quantitative voxel-by-voxel calculated CBV and CBF images. Note that the voxel-by-voxel CBV and CBF values were consistently higher for all regions, and that the percent change in CBF from the ROI analysis to the voxel analysis was the largest for the infarct (68.0%) and penumbra regions (44.6%), while for the normal regions (thalamus, WM, mirror infarct, and mirror penumbra) the maximum percent change was 25%.

Table 4 compares the CBF and CBV values for cortical GM and WM calculated in our study with values found in the literature.Note that the CBF and CBV values calculated using MR bolus tracking techniques are typically larger than the values calculated using other techniques.

The SNR and ζ values of the bolus tracking volumes from the patient shown in Fig. 3 are displayed in Table 5.Note that the SNR depends on which time volume is analyzed (baseline vs. peak signal intensity drop) as well as the region being analyzed. As expected, the infarct ROI demonstrated the least drop in SNR since it had the poorest Gd-DTPA bolus passage, and the ζ values for all regions were close to unity, with the thalamus and infarct regions showing the maximum and minimum values, respectively.

Finally, Figs. 3 and 5 depict two extreme cases from our data. For the case shown in Fig. 3, the MRA showed a complete left anterior cerebral artery occlusion. The initial and final infarct sizes were 57 and 58 cm^3, respectively, and the volume of the penumbra region was 90 cm^3. The CBF, CBV, and MTT values of the infarcted region were 10 ml/min/100 g, 5%, and 28.5 seconds, respectively, and for the penumbra region they were 31 ml/min/100 g, 8.9%, and 17.3 seconds, respectively. Note that very little of the penumbra region became infarcted.

For the case shown in Fig. 5, the FLAIR images acquired 5 days after stroke onset showed an enormous increase (241%) of infarcted tissue. The MRA images depicted a left internal carotid artery occlusion with collateral circulation through the anterior communicating artery. This case was unusual because the penumbra as depicted by the MTT images was much smaller than the final infarct size (180 cm^3 vs 266 cm^3). The CBF, CBV, and MTT values for the initial infarct were 8.5 ml/min/100 g, 2.8%, and 19.4 seconds, respectively, and for the surrounding tissue that later became infarcted (the difference between the white ROI and the red ROI as shown in Fig. 5), the values were 21 ml/min/100 g, 5.8%, and 16.8 seconds. In the region just rostral to the initial infarcted region that did not show abnormal MTT values but later became infarcted (see the FLAIR images in Fig. 5), the CBF, CBV, and MTT values were 44.0 ml/min/100 g, 6.9%, and 9.4 seconds, respectively, and for the corresponding mirror region the values were 49.3 ml/min/100 g, 6.4%, and 7.8 seconds. Therefore, this region was probably not affected by the initial stroke. We suspect that either the patient

Table 1
Summary Statistics (N = 40) for the Four Sets of AIFs Calculated by the Different Radiologists

Radiologist	Avg. height threshold (%)	Avg. peak time (sec)	Avg. area (arib. units)	Avg. no. of voxels
T.D.	69 ± 8	15.6 ± 5.3	14.6 ± 2.1	11.2 ± 2.5
G.C.	66 ± 7	15.6 ± 4.8	13.5 ± 2.9	8.0 ± 3.0
C.G.	65 ± 1	15.0 ± 4.9	13.2 ± 2.4	9.1 ± 1.8
F.M.	64 ± 9	15.0 ± 4.7	13.4 ± 2.4	9.3 ± 1.7

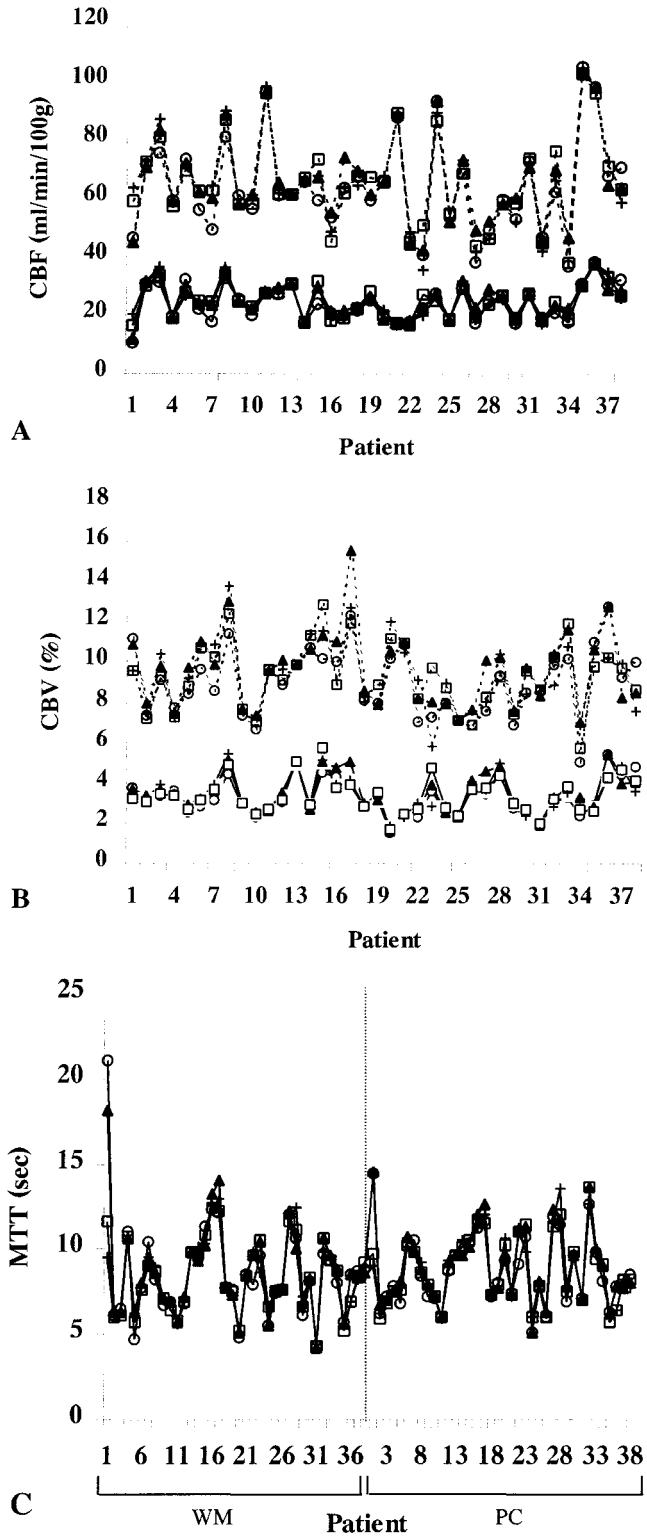

Figure 4. **A:** CBF for parietal cortex (broken line) and WM (solid line) regions for the four different AIFs calculated by the different radiologists (circles, T.D.; plus marks, G.C.; triangles, C.G.; squares, F.M.). **B:** CBV for parietal cortex (top) and WM regions (bottom) using same symbols as in A. **C:** MTT (calculated using Eq. [5]) for WM and parietal cortex (PC) regions. The WM values are plotted first for each patient (the first set of 38 numbers) followed by the PC values. The dotted line represents the boundary between the WM and PC regions. Note that there is not a big difference between PC and WM MTT values.

had a general decrease of perfusion pressure, causing the collateral circulation to no longer supply enough blood to this region or that an embolus from the internal carotid occluded the left middle cerebral artery sometime after the acquisition of the perfusion images (no follow-up angiography was performed).

In the vast majority of cases, the penumbra as defined on the MTT image was always larger than the final infarct size, and hence the penumbra could be separated into two classes: tissue that went on to become infarcted and tissue that remained viable. One preliminary result from our data was that whenever the CBF value of the penumbra was below 18 ml/min/100 g, the tissue always became infarcted (20).

DISCUSSION

The methodology was presented for implementing indicator dilution theory for whole brain quantitative CBF, CBV, and MTT measurements. The CBF and CBV values of GM and WM agreed well with those previously reported in the MR bolus tracking literature for two slice acquisitions (1,3). The CBF and CBV values calculated using the different AIF curves generated by four independent users were not significantly different. The MTT values from unaffected regions were not significantly different from each other, whereas the MTT values from the affected regions (infarct and penumbra) were significantly different from the WM MTT values. The infarct and penumbra CBV values were not significantly different from their corresponding mirror values, but the MTT and CBF values were. Finally, calculating the CBF and CBV on a voxel-by-voxel basis and then drawing an ROI and calculating the mean CBF and CBV did not always give the same results as forming an average tissue curve and then calculating the CBF and CBV.

The only user-dependent step in the methodology, that of finding the voxels to calculate the AIF curve, was shown to be user independent and typically took 5–10 minutes for a trained radiologist. Note that this technique was implemented using gradient-echo T2*-weighted volumes. Spin-echo EPI volumes do not give the same results (12) since the susceptibility contrast of large vessels is smaller than that of small vessels (13) and may have been the reason why Østergaard et al (2) used an empirical constant to convert their MRI measured values to the positron emission tomography (PET) values. Our group is currently analyzing and comparing results from bolus tracking data acquired from the principles of echo-shifting with a train of observations (PRESTO, 21) sequence as well.

Although the CBF and CBV values for GM and WM regions were similar to those measured with MR bolus tracking techniques (1,3), the MR values tended to be larger than those reported in the PET and CT literature. A possible explanation may be that the AIF is underestimated when using MR bolus tracking techniques, which would cause overestimation of both the CBF and CBV values. Underestimation of the AIF may occur for four reasons. First, the resolution and methodology differences may bias the values differently for each system or method used. Second, the constant K in Eq. [1] may

Table 2
Averages and Standard Deviations of CBF, CBV, and MTT for Six Different Regions

	Thalamus (n = 38)	WM (n = 38)	Infarct (n = 34)	Mirror infarct (n = 34)	Penumbra (n = 28)	Mirror penumbra (n = 28)
CBF (ml/min/100 g)	69.8 ± 22.2[a]	28.1 ± 6.9	34.4 ± 22.4[b]	60.3 ± 20.7	50.2 ± 17.5[b]	64.2 ± 17.0
CBV (%)	9.0 ± 3.0[a]	3.9 ± 1.2	7.1 ± 2.7	8.2 ± 2.3	10.4 ± 2.4	9.5 ± 2.3
MTT (sec)	8.0 ± 2.1	8.6 ± 3.0	16.1 ± 8.9[b,c]	8.6 ± 2.9	13.3 ± 3.5[b,c]	9.4 ± 3.2

[a]Significantly different from the corresponding WM value ($P < 0.01$).
[b]Significantly different from the corresponding mirror value ($P < 0.01$).
[c]Significantly different from the WM MTT value ($P < 0.01$, corrected for multiple tests).

not be the same for large arteries compared with small vessels and capillaries even for T2*-weighted gradient-echo EPI images (as discussed in the above paragraph). Third, the value of κ in Eq. [4] may have been too large, meaning either that the chosen value for HCT_{SV} was too large, or the chosen value for HCT_{LV} was too small, or both. In addition, the value of κ is not likely to be the same across patients or even within the same patient. Finally, the voxels selected to represent the AIF may still have partial volume effects with the surrounding tissue. The later may be corrected by calculating a venous output function (VOF) in the same manner that the AIF was calculated in this study, except now the user should look for delayed large peaks and voxels located near large veins and the sinuses. The AIF can be scaled such that the integral equals that of the VOF (this is true due to the conservation of mass) (7).

No significant differences were found among the MTT values of normal regions (GM, WM, mirror infarct, and mirror penumbra), whereas the values were significantly delayed in the infarcted and penumbra regions with respect to the WM values. The MTT may therefore be a good marker of perfusion defects since it is relatively homogenous in normal flow regions, whereas CBF and CBV values vary in normal flow regions (eg, WM and GM).

The CBF and MTT values in the infarcted and penumbra regions were significantly different from their corresponding mirror regions, but not the CBV values. The CBV values measured in infarcted regions have been reported to decrease, increase (due to vasodilation of small vessels and recruitment of capillaries), or remain unchanged, depending on the perfusion pressure, time from stroke onset, and where the stroke occurred (22–26). Since we averaged over all patients and did not try to classify the patients into subgroups, it was not surprising that the average CBV values for the affected regions were not significantly different from their corresponding mirror regions. Therefore, it is important that measures of CBF and MTT be made in addition to CBV measures when analyzing bolus tracking data acquired from patients with suspected stroke.

A consistent agreement was not found between calculating the CBF and CBV on a voxel-by-voxel basis and then drawing an ROI versus calculating the average $C_m(t)$ curve from the ROI and then calculating the CBF and CBV, especially in the infracted and penumbra regions. One reason may be that those voxels whose time curve could not be fit by a gamma variate function were excluded when calculating the mean CBV and CBF values, which would have increased the mean values compared with their corresponding ROI analysis values. Another reason, as mentioned by Østergaard et al (27), is that there is probably not a high enough SNR on a voxel-by-voxel basis to form quantitative CBF and CBV maps. Smoothing the images spatially would of course improve the SNR at the expense of resolution and may allow for a voxel-by-voxel calculation. Also note that no error bars were estimated on the parameters calculated from an average $C_m(t)$ curve. Although the errors can be estimated on the gamma variate fit by using the curvature matrix calculated during the fitting process, these errors must be propagated through the deconvolution process (Eq. [3]) in order to be able to estimate the errors on the CBF, CBV, and MTT values. The most practical way to do this would be to employ Monte Carlo techniques, which would increase the processing time considerably and therefore was not done in this study.

When calculating CBF, CBV, and MTT on an ROI basis, the result was almost instantaneous once the AIF had been calculated, whereas ≈25 minutes were needed for a voxel-by-voxel calculation (due to the fact

Table 3
Comparison of CBV and CBF Values Calculated Either From a ROI Analysis, or the Same ROI Placed on the Calculated CBV and CBF Volumes (n = 10)*

Analysis	Thalamus	WM	Infarct	Mirror infarct	Penumbra	Mirror penumbra
ROI						
CBV (%)	9.1 ± 3.0	3.7 ± 1.1	7.3 ± 2.7	8.0 ± 2.0	10.5 ± 1.8	9.6 ± 1.8
CBF (ml/min/100 g)	72.6 ± 18.1	28.4 ± 8.9	30.4 ± 21.5	63.2 ± 20.4	44.1 ± 13.2	66.8 ± 14.0
Voxel						
CBV (%)	10.2 ± 3.1	4.1 ± 0.6	9.5 ± 3.4	9.6 ± 2.7	11.8 ± 2.1	11.0 ± 1.5
CBF (ml/min/100 g)	81.7 ± 22.4	34.3 ± 9.2	51.1 ± 21.7	79.3 ± 26.8	63.8 ± 16.9	83.7 ± 16.9

*Mean ± standard deviation. All voxel analysis CBV and CBF region values were significantly different from their corresponding ROI analysis values except for the WM CBV region (paired t-test, $P < 0.05$).

Table 4
Comparison of CBF and CBV Values From This Study and Literature Values*

Reference	Study type	GM CBF (ml/min/100 g)	GM CBV (%)	WM CBF (ml/min/100 g)	WM CBV (%)
Present study	MR bolus	65.5 ± 16.3	9.6 ± 1.9	28.1 ± 6.9	3.9 ± 1.2
1	MR bolus	69.7 ± 29.7	8.0 ± 3.1	33.6 ± 11.5	4.2 ± 0.9
3	MR bolus	52.2 ± 16.4	—	27.4 ± 6.8	—
28	MR ST	81.0 ± 20.0	—	23.0 ± 7.0	—
29	MR ST	58.5 ± 7.2	—	20.7 ± 2.3	—
30	PET	65.3 ± 11.0	—	21.4 ± 9.0	—
31	PET	—	5.0 ± 0.7	—	3.5 ± 0.2
32	PET	42.0 ± 8.0	3.8 ± 0.5	22.2 ± 4.9	2.7 ± 0.6
33	CT	—	4.5 ± 0.6	—	2.5 ± 0.6

*(CT = computed tomography, ST = spin tagging technique). The GM ROI in the present study was drawn in the parietal cortex; when possible, a similar region was chosen from the literature. No age matching of the CBF GM values was done.

that a gamma variate fit must be performed for each voxel) on the workstation used in this study. We were able to decrease this processing time to 5–10 minutes (limiting step is time needed to calculate the AIF) by nonquantitatively calculating the CBV and MTT maps by either not using a voxel-by-voxel gamma variate fit in our program or using the commercial software Functool® (General Electric). Our data analysis software can be integrated into the Advantage Windows® workstation browser (General Electric), thus allowing the mean transit time and negative enhancement integral (proportional to CBV) volumes calculated by Functool® as well as the trace diffusion and bolus tracking volumes to be loaded into the program by selectioning the various images in the browser. ROIs can then be drawn on these volumes for regional quantitative CBF, CBV, and MTT calculation.

Ideally, more time volumes should be acquired to allow a better estimation of the baseline as well as allow the Gd-DTPA concentration to return to baseline. A previous study concluded that single-slice nonquantitative CBV maps calculated using 10 baseline images with $\zeta = 1.2$ had 34% more noise than those calculated using 50 baseline points (19). In our study, we used only 3 baseline points (and only 2 for one patient with an early bolus), and our value for ζ was also about 1.2, suggesting that a poor estimate of the baseline signal may be introducing a large variance in our estimated parameters. Figure 4 may give some idea as to how much variance was present in the CBF and CBV estimates by looking at these values for the WM ROI from all 38 patients (mean ± standard deviation: CBF 28.1 ± 6.9 ml/min/100 g, CBV 3.9 ±1.2%). The CBF and CBV values for WM regions are generally considered to be less variable among different subjects than GM regions. The physiologic variances from one patient to another are of course included in these figures. In this present study, we were unable to acquire more time volumes due to a manufacturer's software limitation as to how many total volumes could be acquired. Had we been able to acquire more volumes, the data from two of the patients in this study would not have been excluded. Current versions and other manufacturers' software may not have this limitation, and therefore future studies should acquire more volumes. If the numbers of volumes are limited, patients with cardiac disorders should have the bolus of Gd-DTPA injected several seconds before the start of the image acquisition.

We are currently analyzing all the cases in this paper as well as additional cases to determine whether the absolute values of CBF, CBV, and MTT may be useful for predicting penumbra that will evolve to become infarcted tissue. Note that for a thorough 3D quantitative analysis of the penumbra, whole brain or at least multislice acquisition of bolus tracking volumes must be performed. Many sites already acquire whole brain acquisitions and perform nonquantitative analysis on the images, and the technique presented in this paper puts no extra burden on the data acquisition [other than that the EPI sequence needs to be a gradient-echo sequence, not a spin-echo sequence, as discussed above (12)] only on the data processing. A quantitative analysis is especially interesting because if correlations do exist between the CBF, CBV, and/or MTT absolute values and penumbra that evolves to become infarcted, than

Table 5
SNR Values of Baseline (2nd Acquired Volume) and Bolus Tracking Volume That Contained Peak Signal Drop for the Given ROI, From the Case Shown in Fig. 3*

	Thalamus	WM	Infarct	Mirror infarct	Penumbra	Mirror penumbra
SNR baseline	148	130	139	141	136	139
SNR peak bolus	120	117	131	121	118	107
Δ%	−19	−10	−5.8	−14	−13	−23
ζ	1.21	1.09	1.07	1.20	1.19	1.24

*Δ% is the percent SNR change from the baseline volume to peak bolus volume. The value ζ is also given (see Eq. [8]).

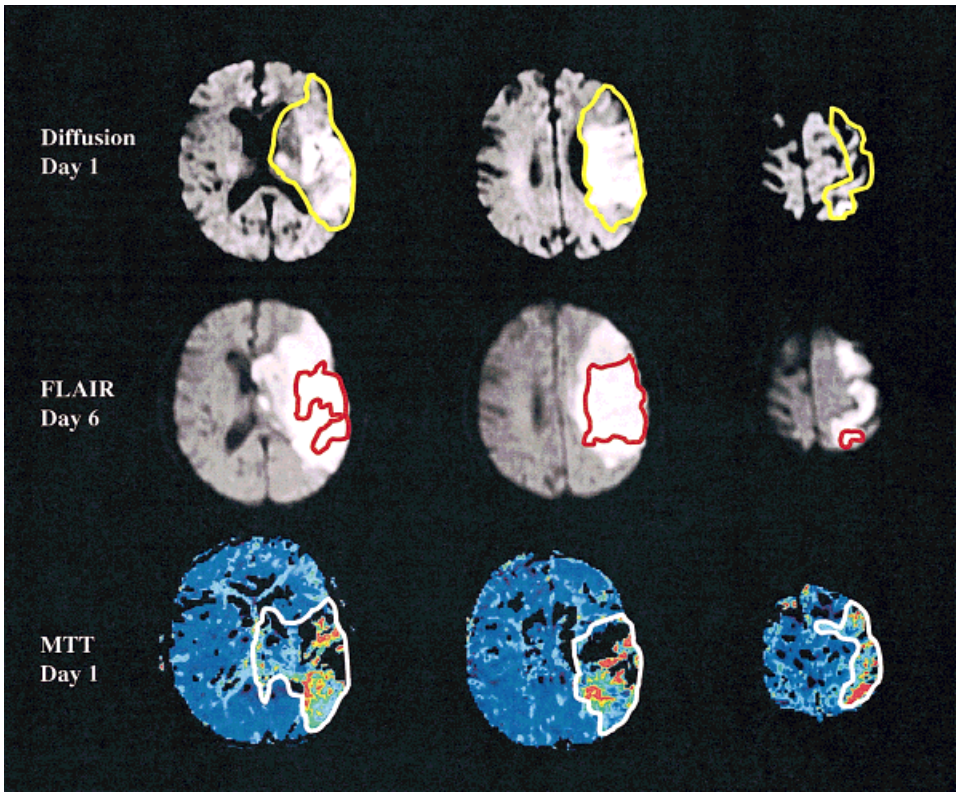

Figure 5. Top row: Diffusion images acquired within 6 hours of stroke symptom onset. The yellow ROI (corrected for ventricular edema) depicts infarct size 5 days later (266 cm^3) as drawn on the FLAIR images from middle row. Middle row: FLAIR images acquired 5 days later. Red ROI depicts infarct size (78 cm^3) as drawn on initial diffusion images (top row). Bottom row: MTT images calculated from data collected within 6 hours of stroke onset. White ROI (180 cm^3) depicts the regions with abnormal MTT values compared to the contralateral mirror region. The size of the penumbra region (white ROI - red ROI) was 102 cm^3. Note that the final infarct size was even larger than the penumbra as defined by the MTT images and that in order to study the full extent of the penumbra and infarct regions, a multislice or whole brain acquisition was needed when acquiring the bolus tracking images. Not all slices containing the infarct and penumbra are shown.

these parameters will be useful on a clinical basis for decisions regarding stroke patient management. The clinical relevance of these results and its impact on hyperacute stroke management are currently being analyzed and will be reported at a later date.

One drawback of this study was that there were no other independent measures of CBF or CBV to verify our technique. We are currently undertaking a study that will compare the regional CBF and CBV values of normal volunteers measured using our technique with those measured using PET. We will also draw arterial blood samples during the Gd-DTPA bolus injection and compare this AIF with that measured from the MRI images to be sure we are obtaining an accurate AIF with our technique.

CONCLUSIONS

A quantitative whole brain bolus tracking technique for gradient-echo EPI images was implemented and shown to have minimal interuser variance. The values calculated for CBF and CBV in normal WM and cortical GM were in agreement with previous results reported in the MR bolus tracking literature and were slightly higher than those reported in the PET literature. The average values for infarct and penumbra CBV were not significantly different from their corresponding mirror values in 38 hyperacute stroke patients, whereas the CBF and MTT values were significantly different. This finding emphasizes the importance of measuring CBF and MTT in addition to CBV in patients with suspected stroke.

ACKNOWLEDGMENTS

The authors thank Christian Michel and Grant Gullberg for useful discussions.

REFERENCES

1. Rempp KA, Brix B, Wenz F, et al. Quantification of regional cerebral blood flow and volume with dynamic susceptibility contrast-enhanced MR imaging. Radiology 1994;193:637–641.
2. Østergaard L, Smith DF, Vestergaard-Poulsen P, et al. Absolute cerebral blood flow and blood volume measured by magnetic resonance imaging bolus tracking: comparison with positron emission tomography values. J Cereb Blood Flow Metab 1998;18:425–432.
3. Hagen T, Bartylla K, Piepgras U. Correlation of regional cerebral blood flow measured by stable xenon CT and perfusion MRI. J Comput Assist Tomogr 1999;23:257–264.
4. Petrella JR, DeCarli C, Dagli M, et al. Assessment of whole-brain vasodilatory capacity with acetazolamide challenge at 1.5 T using dynamic contrast imaging with frequency-shifted BURST. AJNR 1997;18:1153–1161.
5. Meier P, Zierler LL. On the theory of the indicator-dilution method

for measurement of blood flow and volume. J Appl Physiol 1954;6: 731–744.
6. Zierler KL. Theoretical basis of indicator-dilution methods for measuring flow and volume. Circ Res 1962;10:393–407.
7. Axel L. Cerebral blood flow determination by rapid-sequence computed tomography. Radiology 1980;137:679–686.
8. Rosen BR, Belliveau JW, Buchbinder BR, et al. Contrast agent and cerebral hemodynamics. Magn Reson Med 1991;19:285–292.
9. Moseley ME, Vexler Z, Asgari HS, et al. Comparison of Gd- and Dy-chelates for T2* contrast-enhanced imaging. Magn Reson Med 1991;22:259–264.
10. Fisel CR, Ackerman JL, Buxton RB, et al. MR contrast due to microscopically heterogeneous magnetic susceptibility: numerical simulations and applications to cerebral physiology. Magn Reson Med 1991;17:336–347.
11. Kennan RP, Zhong J, Gore JC. Intravascular susceptibility contrast mechanism in tissues. Magn Reson Med 1994;31:9–21.
12. Grandin CB, Smith AM, Mataigne F, Duprez TP, Cosnard G. Quantification of brain perfusion with bolus tracking MRI: comparison of GRE-EPI and SE-EPI. Magn Reson Mater Phys Biol Med 1999;8:8.
13. Weisskoff RM, Zuo CS, Boxerman JL, Rosen BR. Microscopic susceptibility variation and transverse relaxation: theory and experiment. Magn Reson Med 1994;31:601–610.
14. Lassen NA, W. Perl W. In: Tracer kinetic methods in medical physiology. New York, NY: Raven Press; 1979.
15. Press WH, Teukolsky SA, Vetterling WT, Flannery BT. In: Numerical recipes in C. The art of scientific computing, 2nd ed. Cambridge: Oxford: Cambridge University Press; 1992.
16. Marquart DW. An algorithm for least sqares estimation of nonlinear parameters. J Soc Industr Appl Math 1963;11:431–441.
17. Cosnard G, Duprez T, Grandin C, et al. Fast FLAIR sequence for detecting major vascular abnormalities during the hyperacute phase of stroke: a comparison with MR angiography. Neuroradiology 1999;41:342–346.
18. Ostuni JL, Levin RL, Frank JA, DeCarli C. Correspondence of closest gradient voxels: a robust registration algorithm, J Magn Reson Imaging 1997;7:410–415.
19. Boxerman JL, Rosen BR, Weisskoff RM. Signal-to-noise analysis of cerebral blood volume maps from dynamic NMR imaging studies. J Magn Reson Imaging 1997;7:528–537.
20. Cosnard G, Duprez T, Grandin C, et al. Imageries de diffusion et de perfusion en IRM à la phase hyperaiguë d'un accident vasculaire cérébral ischémique. J Radiol 2000 (in press). Volume 81
21. Liu G, Sobering G, Duyn J, Moonen CTW. A functional MRI technique combining principles of echo-shifting with a train of observations (PRESTO). Magn Reson Med 1993;30:764–768.
22. Powers WJ, Raichle ME. Positron emission tomography and its application to the study of cerebrovascular disease in man. Stroke 1985;16:361–376.
23. Baron JC. Pathophysiology of acute cerebral ischemia: PET studies in humans. Cerebrovasc Dis 1991;1:22–31.
24. Kim JH, Shin T, Park JH, et al. Various patterns of perfusion-weighted MR imaging and MR angiographic findings in hyperacute ischemic stroke. AJNR 1999;20:613–620.
25. Hamberg LM, Macfarlane R, Tasdemiroglu E, et al. Measurement of cerebrovascular changes in cats after transient ischemia using dynamic magnetic resonance imaging. Stroke 1993;24:444–450.
26. Maeda M, Itoh S, Ide H, et al. Acute stroke in cats: comparison of dynamic susceptibility-contrast MR imaging with T2- and diffusion-weighted MR imaging. Radiology 1993;189:227–232.
27. Østergaard L, Sorensen AG, Kwong KK, et al. High resolution measurement of cerebral blood flow using intravascular tracer bolus passages. Part II: Experimental comparison and preliminary results. Magn Reson Med 1996;36:726–736.
28. Ye FQ, Mattay VS, Jezzard P, et al. Correction for vascular artifacts in cerebral blood flow values measured by using arterial spin tagging techniques. Magn Res Med 1997;37:226–235.
29. Yang Y, Frank JA, Hou L, et al. Multislice imaging of quantitative cerebral perfusion with pulsed arterial spin-labeling. Magn Res Med 1998;39:825-832.
30. Frackowiak RSJ, Lenzi GL, Jones T, Heather JD. Quantitative measurement of the regional cerebral blood flow and oxygen metabolism in man using ^{15}O and positron emission tomography: theory, procedure, and normal values. J Comput Assist Tomogr 1980;4:727–736.
31. Greenberg JH, Alavi A, Reivich M, Kuhl D, Uzzel B. Local cerebral blood volume response to carbon dioxide in man. Circ Res 1978; 43:324–331.
32. Leenders KL, Perani D, Lammertsma AA, et al. Cerebral blood flow, blood volume and oxygen utilzation: normal values and effect of age. Brain 1990;113:27–47.
33. Hamberg LM, Hunter GJ, Kierstead D, et al. Measurement of cerebral blood volume with subtraction three-dimensional functional CT. AJNR 1996;17:1861–1869.